THE ASTROPHYSICAL JOURNAL, 548:671–680, 2001 February 20

HIGH-RESOLUTION SPECTROSCOPY OF H II GALAXIES: STRUCTURE AND SUPERSONIC LINE WIDTHS

EDUARDO TELLES
Observatório Nacional, Rua José Cristino, 77, 20921-400, Rio de Janeiro, Brazil; etelles@on.br
CASIANA MUÑOZ-TUÑÓN
Instituto de Astrofísica de Canarias, E-38200 La Laguna, Tenerife, Spain; cmt@ll.iac.es
AND
GUILLERMO TENORIO-TAGLE
INAOE, Apartado Postal 51, Puebla, Pue, Mexico; gtt@inaoep.mx
Received 2000 July 13; accepted 2000 October 17

ABSTRACT

We present high-resolution echelle spectroscopy of a sample of H II galaxies. In all galaxies we identify different Hα-emitting knots along the slit crossing the nucleus. All of these have been isolated and separately analyzed through luminosity and size versus σ diagnosis plots. We find that in all cases, for a particular galaxy, the bulk of the emission comes from their main knot and therefore, at least for the compact-class galaxies we are dealing with, luminosity and σ values measured using single-aperture observations would provide results similar to those obtained with spatially resolved spectroscopy. In the size versus σ plots, as expected, there is a shift in the correlations depending on whether we include all emission in a single point or split it into its different emitting knots. The problem of a proper determination of the size of the emitting region so that it can be used to determine the mass of the system remains open. From the data set gathered, using the highest surface brightness points as recently proposed by Fuentes-Masip et al., the best luminosity versus σ correlation turns out to be consistent with a Virial model.

Subject headings: galaxies: ISM — galaxies: kinematics and dynamics — galaxies: starburst — galaxies: structure — H II regions

On-line material: machine-readable tables

1. INTRODUCTION

H II galaxies are a subsample of dwarf galaxies with strong star formation activity leading to intense nebular lines that are easy to detect in objective prism surveys. The optical properties of H II galaxies are dominated by their strong emission-line spectra superposed on a weak blue continuum. The question, posed by Sargent & Searle (1970), of whether these are young galaxies forming stars for the first time seems now to have been answered by recent studies. H II galaxies show an underlying stellar population of intermediate to old ages (Telles & Terlevich 1997; Doublier et al. 1997; Marlowe, Meurer, & Heckman 1999; Cairós et al. 2000). The optical/near-IR colors of their underlying galaxies are similar to late-type dwarf galaxies, although their structural parameters derived from brightness profiles indicate that H II galaxies are more compact than late-type quiescent dwarfs (Telles & Sampson 2000; Telles et al. 1999).

Their morphological classification splits them into two groups: type I includes the most luminous H II galaxies, all of which present an overall irregular morphology. Type II, on the other hand, are more compact and rounder and present a luminosity profile similar to that of dwarf spheroidal galaxies (Telles 1995; Telles, Melnick, & Terlevich). The few H II galaxies found to have a bright neighbor (perhaps by chance) are all type II's of regular morphology, contrary to what one would expect if galaxy interactions could be held responsible for the morphological disturbances found in type I's (Telles & Terlevich 1995). In addition, H II galaxies as a class are not preferentially clustered around faint, low-mass galaxies (Telles & Maddox 2000), but some are found to have H I companions (Taylor 1997). The triggering mechanism of the present starburst in H II galaxies is not at all clear, yet for these dwarfs internal processes must play a major role.

Here we show echelle data obtained at the William Herschell telescope (4.2 m) at the Observatorio del Roque de los Muchachos (ORM) at La Palma on a sample of type II dwarfs. Our high-resolution echelle data show a strong variation in the line profiles across the emitting region, and even in the most compact sources there is an indication of separate knots of star formation (SF) evolving concurrently within the galaxy nucleus. The presence of multiple knots of star formation within the line-emitting regions is also observed on high spatial resolution images, in particular in the near-IR. Telles et al. (1999; and E. Telles et al., in preparation) also identified knots that are possible super stellar clusters (SSC). Their individual properties may impose further constraints on the history of SF of a galaxy as well as indicate possible mechanisms able to trigger the present burst.

For our sample here, we have defined different apertures across the Hα luminosity profile and have extracted the spectra corresponding to different emitting knots in every object. In addition, the "total" spectrum was obtained to mimic single-aperture observations (Melnick, Terlevich, & Moles 1988), when it includes the ensemble of individual knots.

The structure found in H II galaxies has profound implications for several topics, in particular issues such as star formation and its possible sequential propagation in H II galaxies, and how the ISM is structured in these galaxies.

Another issue central in this field of research is the validity of the interpretation, and use of the empirical correlations, of size and luminosity versus their supersonic line widths for high-redshift galaxies. These correlations were first found for giant H II regions by Melnick (1979), Terlevich & Melnick (1981), and Melnick et al. (1987), and extended to H II galaxies by Melnick et al. (1988) and Telles & Terlevich (1993). The fact that giant H II regions and H II galaxies have supersonic motions and follow the same correlations have made us use and refer to the whole ensemble of objects as a single family. This may indicate that the process of massive cluster formation is similar in both H II galaxies and giant H II regions, and it is the main reason we do not differentiate between them in discussing their dynamical properties. In §§ 2 and 3 we describe our selected sample and observational strategy, and § 4 presents full details of the results for each galaxy. A general discussion and a summary of the results is given in § 5.

2. THE OBSERVATIONS

We have carried out long-slit echelle observations of a sample of seven H II galaxies (see Table 1) with the Utrecht Echelle spectrograph at the 4.2 m William Herschel Telescope at the Roque de los Muchachos observatory, La Palma, Spain, on the nights of 1997 May 30–31. Exposures of 1200 s were obtained using a 2148 × 2148 Tek CCD and the 79.0 lines mm^{-1} echelle, reaching typical S/N per pixel of ≥ 30 at Hα. The orders covered are 55 to 30, from ~4130 to 7340 Å, including Hβ and Hα with the short-slit 19″ mode (Mrk 36, UM 461, UM 533, and Mrk 930), and order 34 from ~6500 to 6650 Å on Hα with the long-slit 250″ mode (Mrk 59, II Zw 40, and VII Zw 403). The spectral resolution (FWHM) of our setup was 0.13 Å in the Hβ region and 0.18 Å in the Hα region. This led to a resolution of ~8 km s^{-1}. The CCD frames were reduced using standard procedures with the tasks in IRAF. The data were debiased, trimmed, and flat-fielded using a normalized flat field produced with *apflatten*. The spectra were extracted using *doecslit* with appropriate parameters. Wavelength calibration was performed by using the comparison spectrum of thorium-argon arcs. Flux calibration was accomplished through the observation of standard stars. The atmospheric extinction correction was also applied at the time of calibration using the mean extinction curve for La Palma. The seeing was less than 1″.5.

Table 1 lists the global properties of our selected galaxies. Columns (1) gives the galaxy name. Columns (2) and (3) give their coordinates. Columns (4)–(7) present spectroscopic information from the literature: redshift, Hβ flux, equivalent width of Hβ, and the Balmer decrement (Terlevich et al. 1991).

3. DATA ANALYSIS

Figure 1 displays two panels for each galaxy. The larger left panel shows the direct image from the Digitized Sky Survey (DSS) of a galaxy, while the right smaller panel (alongside the direct image) shows its echelle CCD two-dimensional spectrum. The location and position angle of the slit for our observation are indicated on each direct image. In all cases, the slit was centered on the brightest nucleus, as defined by broadband images. For those galaxies with a compact appearance, the slit was aligned east-west, and for those that displayed a more extended structure, the slit was placed along the "extended" orientation. In the Echelle images, the horizontal direction represent the spatial dimension, while the vertical is the dispersion direction. The image scales are given for both panels. The precise location in relation to the peak intensity is given in Table 2. Note that the spectrum of every subregion has been extracted using variable size apertures covering the extent of the Hα emission. In all cases a large aperture including all the emission detected along the slit in each object has also been defined and is subsequently referred to as the total emission.

The spectral range covered on each spectrum includes Hα (λ6563 Å) and [N II] λλ6583, 6548 Å lines. A clear Hα emission is present in the spectra from all regions in all galaxies; the [N II] doublet, however, only appears in some regions of three galaxies (Mrk 59, II Zw 70, and UM 533). Thus, the analysis presented here is based on the behavior of the Hα emission line of each galaxy.

There is a wide variety of spectral patterns. Some of them display a very well behaved Gaussian Hα line profile; others, however, present clear signs of multiple spectral components. These have been fitted using two (three in the case of II Zw 70) Gaussian templates.

Table 2 lists the derived properties of the spectra of each of the recognized knots or regions, as well as the total for each galaxy. Column (1) gives the galaxy name. Column (2) gives the spatial nomenclature. A clear peak in emission covered by the aperture is referred to as a "knot," while a "region" could represent a zone between knots or an extension. Total emission is the aperture covering all the emission arising from a galaxy. Column (3) gives the rotator position angle of the observation that corresponds to the slit position angle shown in Figure 1. Columns (4)–(5)

TABLE 1

SPECTROSCOPIC DATA FROM TERLEVICH ET AL. (1991)

Name (1)	R.A. (1950) (2)	Decl. (1950) (3)	z (4)	$-\lg F(H\beta)$ (ergs cm^{-2} s^{-1}) (5)	$W(H\beta)$ (Å) (6)	$C(H\beta)$ (7)
Mrk 59	12 56 38.2	35 06 53	0.0027	14.26	17	0.54
II Zw 70	14 48 55.2	35 46 36	0.0040	...	...	0.40
VII Zw 403.....	11 24 35.8	79 16 03	−0.0003	...	...	0.40
Mrk 36	11 02 15.6	29 24 31	0.0022	13.36	70	0.44
UM 461	11 48 59.4	−2 05 41	0.0035	13.20	342	0.40
UM 533	12 57 25.0	2 19 08	0.0030	13.59	101	0.76
Mrk 930	23 29 29.3	28 40 16	0.0181	13.05	71	0.55

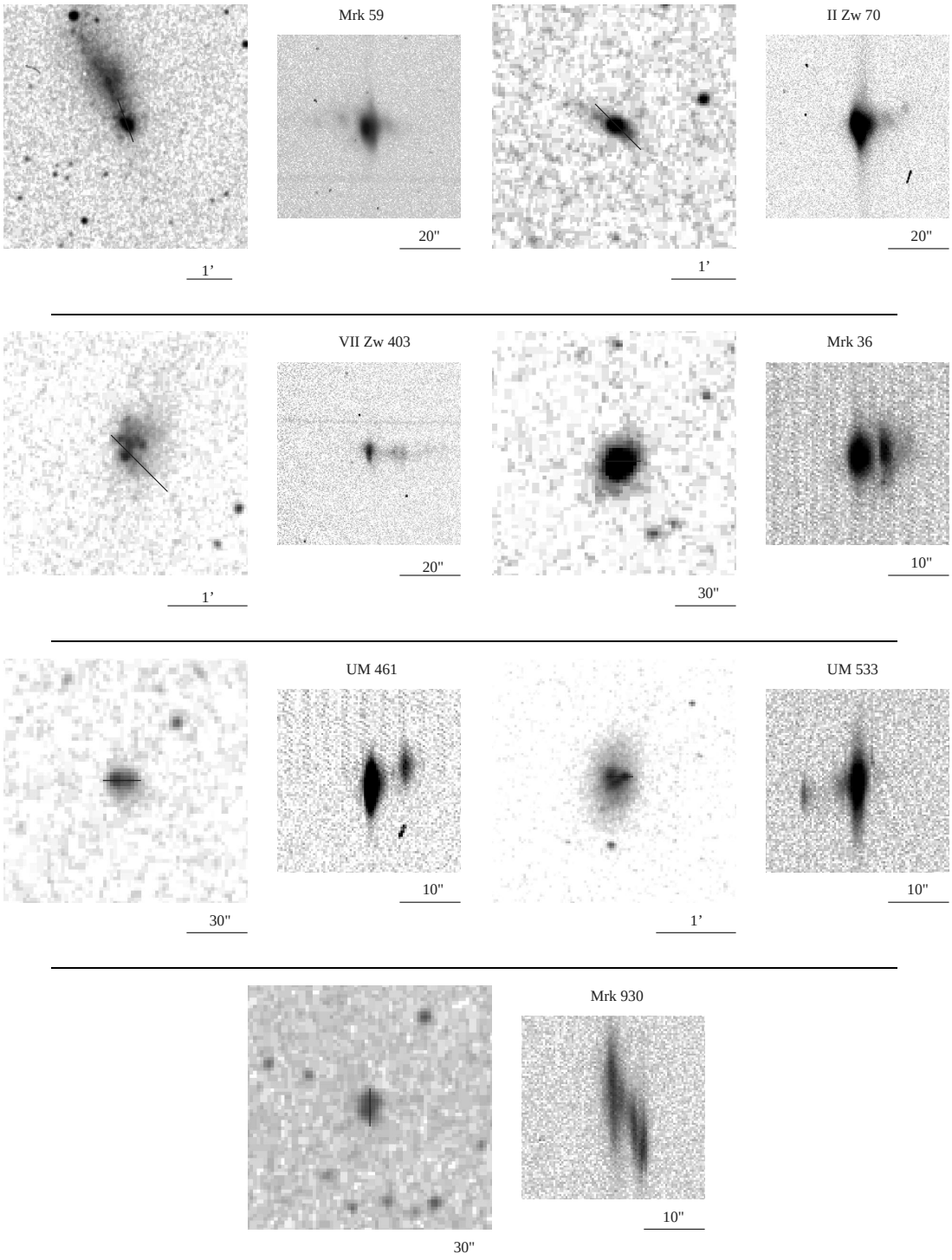

FIG. 1.—*Left larger panels*: Direct image from DSS (north is up, east is left) with slit location indicated. *Right smaller panels*: Echelle CCD image on the Hα spectral region (horizontal is the spatial direction, vertical is the dispersion direction).

provide the aperture position in relation to the main knot and size in arcseconds. Columns (6)–(8) refer to the analysis of the spectra and give the parameters obtained from Gaussian fits to the Hα emission line, namely, Hα flux, central wavelength, and line width (FWHM in Å). The typical errors in flux are 10%–20%, estimated from the sensitivity curves from the standard-star observations and ~5%–10% in line width from the comparison with the Hβ line in the echelle observations or externally with different frames when available. In the cases in which more than one Gaussian is needed to account for the Hα emission line, the table provides the various parameters derived for each of the components. The last column in Table 2 indicates the spectral nomenclature, showing in some cases the presence of the additional spectral components from the emission-line profile and their relative importance. A featureless emission line well fitted by a single Gaussian is referred to as "single," while "global" is a single fit to an emission line

TABLE 2

DERIVED SPECTRAL PROPERTIES

			Aperture					
Name (1)	Knot ID (2)	P.A. (deg) (3)	Position (arcsec) (4)	Size (arcsec) (5)	$F(H\alpha)$ (ergs cm^{-2} s^{-1}) (6)	Peak λ (Å) (7)	FWHM (Å) (8)	Spectral Components (9)
Mrk 59	total	20		30.6	3.356E−13	6580.7	1.190	single
					9.270E−15	6601.4	1.170	single [N II]
	main knot		0.0	10.6	3.710E−13	6580.7	1.173	single
	region 2		−17.6	6.2	3.270E−15	6581.1	0.870	single
	region 3		−8.2	5.2	1.730E−14	6581.2	1.347	global
					1.720E−14	6581.2	1.347	main component
					2.860E−15	6579.8	0.800	secondary component
	region 5		6.1	5.0	1.670E−14	6580.8	1.018	global
					1.590E−14	6580.8	0.960	main component
					2.540E−15	6579.6	1.360	secondary component
II Zw 70	total	45		19.9	2.686E−13	6589.2	1.320	single
					1.550E−14	6610.0	1.800	single [N II]
	main knot		0.0	11.3	2.667E−13	6589.2	1.313	global
					1.680E−13	6589.2	0.850	main component
					4.510E−14	6589.9	1.120	secondary component
					6.000E−14	6588.4	1.020	secondary component
	region 2		10.18	8.6	5.374E−14	6589.2	1.423	global
					4.360E−14	6589.3	1.180	main component
					4.060E−15	6590.5	1.480	secondary component
					9.870E−15	6588.3	1.640	secondary component
	region 3		5.14	7.5	1.695E−14	6589.5	1.437	single
VII Zw 403.....	total	45		18.4	5.650E−14	6560.7	0.980	single
	main knot		0.0	9.7	2.754E−14	6560.7	0.986	single
	knot 2		7.8	3.7	8.938E−15	6560.6	0.829	single
	knot 3		11.1	3.7	4.560E−15	6560.5	1.048	global
					3.960E−15	6560.5	0.900	main component
					4.290E−16	6559.6	0.610	secondary component
	extension		20.7	23.9	7.968E−14	6560.7	1.013	poor S/N
Mrk 36	total	90		15.1	1.650E−13	6577.4	1.108	global
					1.100E−13	6577.4	0.910	main component
					5.840E−14	6577.4	1.870	low-intensity wings
	main knot		0.0	8.1	1.115E−13	6577.4	1.036	global
					9.040E−14	6577.4	0.920	main component
					2.640E−14	6577.4	2.270	low-intensity wings
	knot 2		4.3	4.0	4.721E−14	6577.5	1.336	single
	extension		7.9	5.0	1.129E−14	6577.6	1.373	global
UM 461	total	90		11.4	2.085E−13	6586.1	0.906	single
	main knot		0.0	6.1	1.938E−13	6586.1	0.905	single
	knot 2		5.6	4.4	1.449E−14	6586.8	0.870	single
UM 533	total		90	14.8	1.309E−13	6582.8	1.263	global
					1.190E−13	6582.8	1.130	main component
					1.350E−14	6581.6	1.180	low-intensity wings
					7.260E−15	6603.5	0.960	[N II]
	main knot		0.0	7.4	1.146E−13	6582.7	1.258	single
					6.740E−15	6603.5	1.110	[N II]
	knot 2		−8.7	3.0	6.822E−15	6582.6	0.979	single
	interknots		−4.5	4.4	5.927E−15	6582.3	0.789	single
Mrk 930	total	180		13.4	1.508E−13	6682.1	2.432	single
	main knot		0.0	5.9	8.609E−14	6682.4	2.433	single
	knot 2		1.2	1.7	2.670E−14	6681.9	1.703	single
	knot 3		3.2	2.0	4.197E−14	6681.1	1.679	single
	knot 4		4.8	2.0	3.150E−14	6680.7	1.494	global
					2.316E−14	6680.5	1.160	main component
					8.574E−15	6681.5	1.460	secondary component

NOTE.—Table 2 is also avalable in machine-readable form in the electronic edition of the *Astrophysical Journal*.

that shows more than one resolved component. This would mimic an observation with poorer spectral resolution. The main and secondary components of an emission line were also fitted whenever they arose.

The global (or single) Gaussian fit is a very good representation of the total Hα line profile in the spectrum of a galaxy, as shown in Figure 2. The results of the fit can be compared with parameters traditionally used to analyze the

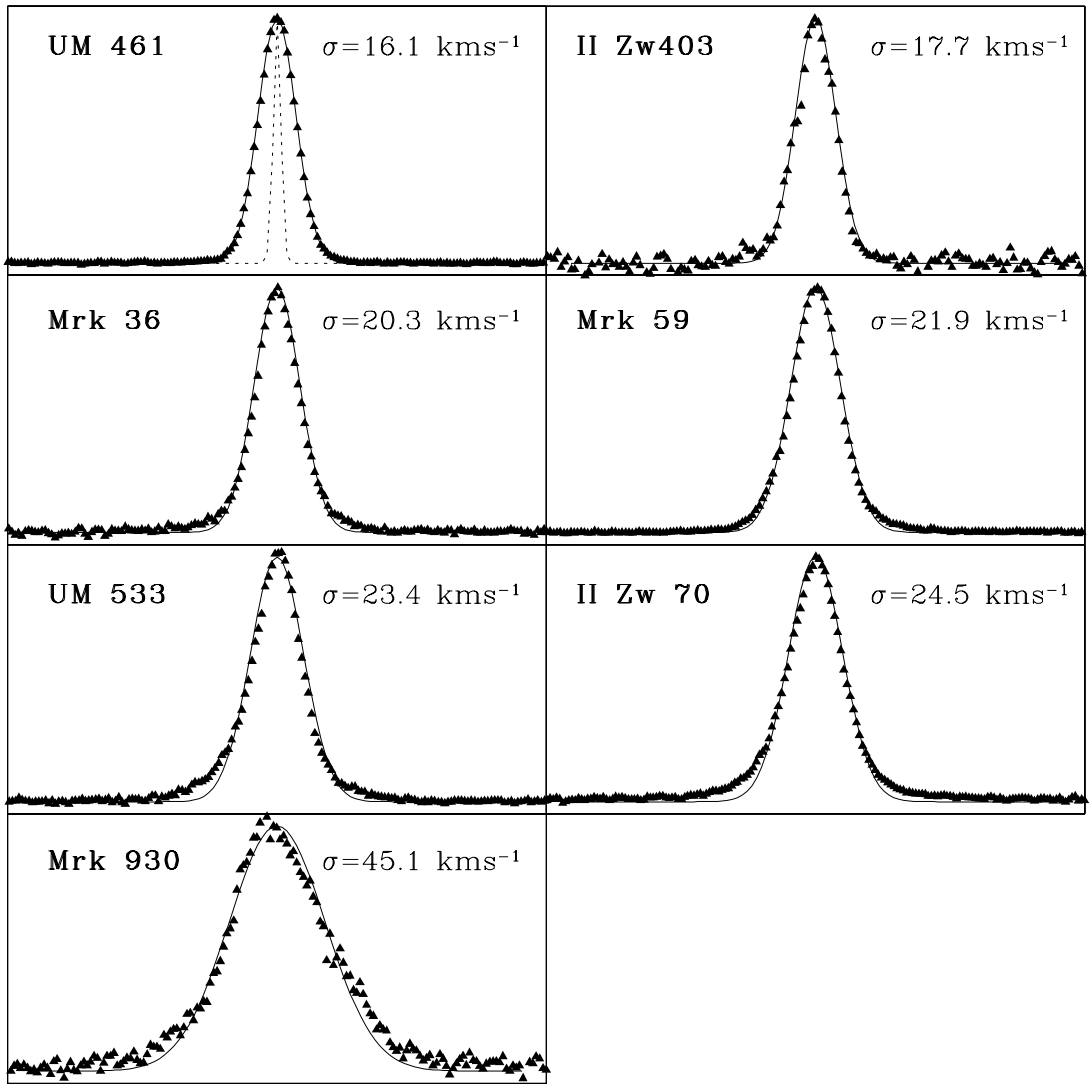

FIG. 2.—Emission-line profiles of H II galaxies covering a 10 Å range centered on the Hα line. Also shown are the Gaussian fits (*solid lines*) used to derive the final gas velocity widths, which are given in the top right of each panel and listed in Table 3. The comparison thorium lamp line profile is shown in the first panel, upper left, by a dotted line.

kinematics of H II regions using single-aperture spectroscopy (see Melnick et al. 1988; Muñoz-Tuñón 1994 and references therein).

4. RESULTS

Here we briefly describe the most general spectral features found in each galaxy of the sample. The qualitative description of each of these features is based on the precise measurements, i.e., the emission-line parameters, given in Table 2.

From our results in Table 2, it is clear that even the apparently most compact of our H II galaxies (e.g., UM 461, which spans across 11″) splits into several components, or emitting knots. Some of these may be true centers of stellar formation, but others could simply be high-density condensations ionized from the outside by the stellar radiation.

The emitting knots in every galaxy present different properties (intensity, line width, etc.); however, in all cases the velocity dispersion extracted from the total fit to the spectra of every galaxy is, within the errors, identical to the velocity dispersion inferred for the main emitting knot found in every galaxy. This is a result now well established in the field of giant H II regions (e.g., Muñoz-Tuñon 1994; Sabalisck et al. 1995; Muñoz-Tuñon et al. 1995). In the seven galaxies in our sample, the main knot peak intensity amounts to half, or more, of the total intensity derived for the total fit. The other main components of other knots, in every galaxy, amount to less than an order of magnitude of the peak intensity of the total fit, and in many cases their line width is smaller than that derived for the main emitting knot. This is also the case for all secondary components required to fit low-intensity line asymmetries, or shoulders, although the peak intensity of these lines is usually much smaller. On the other hand, the secondary components required to fit the wing emission of some of the knots in every galaxy contribute by much less than an order of magnitude to the total emission and are in all cases very broad lines, with line width values well above the value measured for the main emitting knot. Note, however, that uncertainties in the fit to low-intensity wings are much larger.

Thus, the line-emitting properties of H II galaxies, including their supersonic σ value, are in all our cases dominated

by the emitting properties of the most intense knot. Thus, similar to the case of giant H II regions, it seems that the main emitting knot reflects an intrinsic property generated by the recent starburst event (see Tenorio-Tagle et al. 1993; Muñoz-Tuñon et al. 1996).

4.1. *Notes on Individual Objects*

4.1.1. *Mrk 59*

Mrk 59 has a northeast-southwest oriented "comet-like" optical appearance (see Fig. 1). More recent studies have paid special attention to this subclass of H II galaxies (see Noeske et al. 2000). It shows a conspicuous bright region, which clearly dominates the emission, located at the tip of an extended tail. The optical nucleus contains a rich substructure in nebular emission. We have defined five subregions in total. However, a clear peak in luminosity (main knot) is identified with a size (measured on the baseline of the Hα line spatial profile) of $\sim 10''$. At a much lower intensity level, there is an extended emission centered at $\sim 7''$ from the main knot. In a similar way, we have identified other intensity peaks showing emission along the slit, which we named regions 2 and 3. In this galaxy the main knot intensity totally dominates the output of the emitting region.

4.1.2. *II Zw 70*

This is a very compact dwarf. Its image displays a single optical knot with some "disklike" extended emission in the broad band (see Fig. 1). On the long-slit echelle CCD frame, one can see a clearly defined Hα line as well as the [N II] doublet. The nebular emission spatial distribution is almost pointlike, with a slight asymmetry presenting an extended, lower intensity Hα emission. The nebular luminosity profile led us to define three apertures, from which we have extracted and analyzed the spectra. We refer to these as the main knot (which overwhelmingly dominates the emission), region 2, and region 3. The Hα emission line in the three apertures presents a remarkably symmetric profile, which, however, cannot be well fitted by a single Gaussian, due to the presence of low-intensity wings. In fact, a minimum of three Gaussians are needed to obtain a good fit. The values derived for the three components are given in Table 2.

4.1.3. *VII Zw 403*

This is a classical example of a very nearby blue compact galaxy. Its broadband optical morphology presents a typical core-halo structure with an extended light distribution. It has been the target of the *Hubble Space Telescope* (*HST*) for studies of its stellar content (Schulte-Ladbeck et al. 1999a, 1999b). The distance to VII Zw 403 derived from these studies, and adopted here, is 4.4 Mpc.

From our data, we have identified along the slit a clear peak in emission: the main knot, which produces half the luminosity of the galaxy. The spectrum of the main knot is well fitted by a single Gaussian, with the possible presence of low-intensity wings, too weak to be modeled. No signs of line splitting are seen at our present spectral resolution. In addition to the main knot there are two additional intensity maxima (knots 2 and 3) very close to each other. The spectrum from knot 2 displays a Gaussian-like Hα line. On knot 3, however, there seems to be a secondary component. The line can be reproduced using two Gaussians, very close in wavelength (less than 1 Å). Moving along the slit, immediately behind the two secondary knots one finds an extended emission (called "extension" in Table 2), which, despite the poor S/N, we have fitted using a Gaussian, with parameters similar to those obtained from the fit to the total spectrum of the galaxy.

4.1.4. *Mrk 36*

Our echelle observations were taken with the slit oriented east-west (P.A. = 90°) crossing the optical core of the galaxy. This object has been of particular interest because it shows a very "blobby" structure, most visible in near-IR images (Telles et al. 1999; E. Telles et al., in preparation). However, our present observation crosses the bright nucleus, which, as described below, also presents a well-resolved structure. Bidimensional spectroscopy with integral field units will be very valuable in the near future to unveil its internal kinematics and help us answer the question of the origin of the present starburst.

From the luminosity profile across the slit, we have identified two main peaks of nebular emission (see Fig. 1), labeled as the main knot (the brightest one) and knot 2. Two more apertures have been defined for the analysis; the "total," which includes the whole emission from the galaxy, and an "extension," which rescues the extended, low-intensity emission in addition to knot 2.

The main knot shows the dominant Hα emission component. For the fitting to also be successful at the base of the line (low-intensity wings), a second Gaussian is needed. This has a much lower intensity, but it is broader than the main component. The parameters obtained from doing the fitting with only one Gaussian are also presented on Table 2 and are referred to as "global." The secondary, low-intensity broad component is also present in the integrated (total) spectrum, which is clearly dominated by the emission from the brightest main knot.

4.1.5. *UM 461*

UM 461 appears along the slit as a pointlike source (see Fig. 1). We extracted its spectra from an aperture covering the main knot. A secondary, much weaker second peak west of the main knot was also detected (knot 2). To compare the line profiles with those obtained using a single-aperture spectrum, a third aperture covering all emission has been taken (the "total"). The Hα emission from the three apertures can be nicely fitted with a single Gaussian profile. The main knot dominates the total nebular emission of the galaxy, and therefore the spectra from the main knot and the total are rather similar. It is important to note that the second weak knot (knot 2), although clearly spatially separated from the main one, shares its main kinematic parameters (see Table 2).

4.1.6. *UM 533*

Its optical appearance, as seen at the DSS, is that of a halo engulfing a heartlike core with two clearly visible nuclei. Our slit was positioned in the east-west direction (P.A. = 90°) crossing the two nuclei. First thing to note (see Fig. 1) is that these two peaks are also visible in nebular emission. There the contrast is much larger, with a clear bright knot (main knot) and a much weaker one separated by about 10″ (knot 2). To make a comparison and to find the spatial trend of the emission lines, two more apertures were defined: an aperture covering the region in between knots 1 and 2 (interknots) and an aperture including the whole emitting region ("total"). In this galaxy, [N II] (6583

Å) is also detected in the bright knot. The Hα emission of the brightest knot shows a good Gaussian behavior on the line core; however, at least a second Gaussian is needed to account for the emission arising from the line base. Low-intensity wings are also evident on the spectra covering the whole emission, which, as mentioned before, is dominated by the brightest knot.

4.1.7. *Mrk 930*

This galaxy presents the largest redshift ($z = 0.018$) of our sample. It has a knotty appearance on the broadband image, and its nebular emission along the slit (located north-south, P.A. = 180°) also displays a multiple-knot structure. At the same time, the ensemble of knots seems to show a velocity trend (see Fig. 1). From the luminosity profile, four apertures were selected, centered on each of the emission peaks (knots). The spectra from all of them are well reproduced with a single Gaussian profile, whose parameters are given in Table 2. The total spectrum, with a spatial beam of 14″, covering all the emission, is also Gaussian-like, and presents the same σ value detected in the main knot. The main knot also accounts in this case for more than half of the total emission from the galaxy.

4.2. *Structural Parameters*

Our echelle data have led us to built a comprehensive database of sizes, velocity dispersions, and luminosities of the galaxies of our sample; not only of the total parameters, but also for the starburst substructures found in each of them (Table 3).

Table 3 describes the derived physical parameters of our sample. Columns (1) and (2) identify the galaxy and the region or knot as described in Table 2. Column (3) gives values of the velocity dispersion, $\sigma_{\rm gas}$, obtained after correcting the observed line width (given in Table 2) for instrumental and thermal broadening ($\sigma^2_{\rm gas} = \sigma^2_{\rm obs} - \sigma^2_{\rm inst} - \sigma^2_{\rm th}$), assuming a 10^4 K gas. Columns (4) and (5) give the Hα luminosity and the physical "radius" (aperture size/2) of a region or knot in pc. Column (6) gives an estimate of the Hα surface brightness within the slit. Finally, we give derived distances from their observed redshift z (expect for VII Zw 403, as described above). Throughout this paper we use the current value of $H_0 = 65$ km s^{-1} Mpc^{-1} (Suntzeff et al. 1999).

Our high-quality data is here compared to see if it is in agreement with previous statistical works showing that H II galaxies follow the luminosity versus σ ($L \propto \sigma^4$) and size versus σ ($R \propto \sigma^2$) relations. These correlations have often been obtained using single-aperture spectroscopy, and their validity under better spectral and spatial resolution is a key issue to be verified. Note that in each of our galaxies, the difference in the velocity centroids of the various components is in all cases less than 1 Å (from Table 2), and thus the velocity shift between components cannot account on

TABLE 3

PHYSICAL PARAMETERS DERIVED FROM THE SINGLE-GAUSSIAN FITS TO THE Hα LINE

Name (1)	Knot ID (2)	$\sigma_{\rm gas}$ (km s^{-1}) (3)	log L(Hα) (ergs s^{-1}) (4)	Radius (pc) (5)	log SB (ergs s^{-1} pc^{-2}) (6)	Distance (Mpc) (7)
Mrk 59	total	21.96	40.16	923	34.95	12.4
	main knot	21.62	40.20	318	35.45	12.4
	knot 2	15.37	38.17	190	33.63	
	knot 3	25.11	38.90	163	34.43	
	knot 5	18.46	38.86	153	34.43	
II Zw 70	total	24.51	40.31	889	34.81	18.4
	main knot	24.37	40.31	507	35.05	
	region 2	26.56	39.61	387	34.47	
	region 3	26.84	39.12	339	34.03	
VII Zw 403.....	total	17.76	38.39	196	34.30	4.4
	main knot	17.88	38.08	104	34.26	
	knot 2	14.58	37.59	39	34.19	
	knot 3	19.16	37.30	39	33.90	
	extension	18.44	38.54	255	34.33	
Mrk 36	total	20.32	39.61	372	34.88	10.2
	main knot	18.84	39.44	198	34.98	
	knot 2	24.92	39.07	100	34.91	
	extension	25.66	38.46	126	34.19	
UM 461	total	16.10	40.09	450	35.07	16.2
	main knot	16.08	40.06	238	35.32	
	knot 2	15.34	38.96	177	34.33	
UM 533	total	23.41	40.00	498	35.00	13.9
	main knot	23.31	39.94	248	35.25	
	knot 2	17.64	38.71	101	34.41	
	interknot	13.64	38.64	144	34.19	
Mrk 930	total	45.06	41.48	2729	34.95	83.8
	main knot	45.08	41.23	1197	35.07	
	knot 2	31.21	40.72	341	35.10	
	knot 3	30.76	40.91	407	35.22	
	knot 4	27.21	40.79	405	35.10	

NOTE.—See text for details. We use $H_0 = 65$ km s^{-1} Mpc^{-1}. Table 2 is also avalable in machine-readable form in the electronic edition of the *Astrophysical Journal*.

its own for the velocity dispersion detected in the total spectrum of a galaxy. The velocity dispersion in our data set thus reflects an intrinsic property of each of the components, and in some cases this is indeed supersonic ($\sigma_{\rm gas} > c_{\rm H\,II}$, the sound speed in the ionized gas).

4.2.1. *The [L-σ] Relation*

Figure 3 plots our $L(\mathrm{H}\alpha)$ versus σ for *all* the data from Table 3. The points were derived from single-Gaussian fits to the spectral line of each aperture, labeled "global" or "single" in the last column of Table 2. Measurements inferred from total apertures are shown by filled triangles. Open squares represent the values of the main knot in each galaxy, while filled circles represent other regions or secondary knots. In the plot, the size of the symbols is proportional to their Hα surface brightness (see Table 3).

Clearly, the luminosity of the points representing the main knots (Fig. 3, *open squares*) falls very close to values derived from apertures covering the total extent of the emitting region (*filled triangles*). The implication of this is that the brightest knot in every galaxy almost entirely dominates the total luminosity. In addition, the velocity dispersion inferred for the main knots is almost identical to that derived from the total galactic emission.

A second point to notice is the clear correlation displayed by either the total emitting spectra or the main knots in our sample of galaxies (see Fig. 3 and Table 4). This fit holds for all galaxies in our sample with the exception of VII Zw 403, which presents $\log \sigma \sim 1.25$ and $\log L(\mathrm{H}\alpha) \sim 38$. Based on the work of Fuentes-Masip et al. (2000), in which a thorough analysis of the luminosity and size versus velocity dispersion of the giant H II regions in the large irregular galaxy NGC 4449 led them to realize that the correlations only hold for nebulae with a supersonic line width and a surface brightness above 2×10^{35} ergs s^{-1} pc^{-2}, we excluded this galaxy from our analysis. Note that VII Zw 403 is the galaxy with the lowest surface brightness in the sample. For this reason, we conclude that this object must fall below the threshold for which the relations hold (although the true luminosity threshold value cannot be established here). The surface brightness effect could be related to a second parameter in the relations, again similar to the fundamental plane of elliptical galaxies, as Telles & Terlevich (1993) first attempted to investigate.

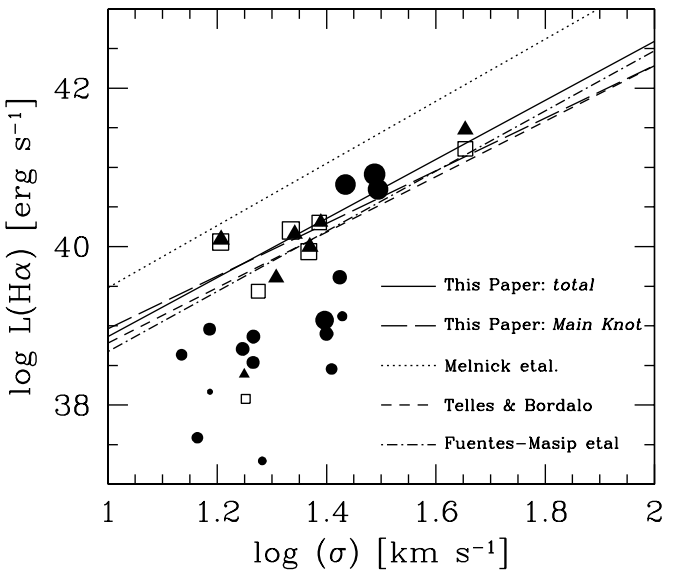

FIG. 3.—Luminosity–line width relation. Symbols show total apertures (*filled triangles*), main knot (*open squares*), and other regions or knots (*filled circles*). Symbol sizes represent relative Hα surface brightness. The lines are simple linear square fits for our data (total: *solid line*; main knot: *long-dashed line*) and statistical works from the literature.

TABLE 4

L-σ SIMPLE LEAST-SQUARE TO TOTAL APERTURE AND GLOBAL LINE FIT VALUES

	$L \propto x \log(\sigma)$		
SOURCE	x	Ξ (ergs s^{-1})	rms
This paper	3.73 ± 1.01	35.14 ± 1.40	0.275
Melnick et al.	3.92 ± 0.47	35.55 ± 0.67	0.426
Telles & Bordalo	3.50 ± 0.67	35.28 ± 1.03	0.539
Fuentes-Masip et al.....	3.80 ± 1.20	34.90 ± 1.70	

NOTE.—Also shown are the relations found from the literature using the same simple linear least-square fit, all transformed to $H_0 = 65$ km s^{-1} Mpc^{-1} as used throughout this paper.

As far as the correlation is concerned (lines in Fig. 3), we note that in our present data either the total (*solid line*) or the main knot (*long-dashed line*) closely agree with the results from other works. The results of Fuentes-Masip et al. (2000) are shown by the dot-dashed line. Telles & Bordalo (in preparation) analyzed a sample of about 40 H II galaxies, and their preliminary results are shown by short-dashed lines. The similarity of these fits is evident in Figure 3. In light of our results, we conclude that irrespective of the structure that a galaxy (or a giant H II region) may have, the main emitting knot is likely to be sitting at the bottom of the gravitational potential well of its host galaxy, and therefore the overall motions are dominated by the mass of the complexes of gas and stars.

The existence of these relations and the presence of a surface brightness effect prompt us to suggest that the L versus σ relation may have an associated second parameter. This issue is being further investigated using two-dimensional spectroscopy.

The numerical results of the various fits are shown in Table 4. Note, however, that the slope of the original Melnick et al. (1988) (L versus σ) relation is virtually identical to all the others, although there is a clear offset on the zero point of their correlation after all appropriate transformations are applied. This could be due to a systematic error in the calibration of their data, since independent calibration of Telles & Bordalo (in preparation) for a statistically significant sample of H II galaxies and the redshift-independent zero points given by Fuentes-Masip et al. (2000) and Bosch (1999) for giant H II regions all agree with the zero point measured here within the uncertainties.

4.2.2. *The [R-σ] Relation*

Figure 4 shows the R versus σ relation for our present sample of H II galaxies. Again, measurements from total apertures are shown by filled triangles. Open squares represent the values for the main knots, while filled circles show other regions or knots. The sizes of the points are proportional to their corresponding Hα surface brightness, as given in Table 3.

From the analysis of this plot and the peak λ of all regions from Table 2, we conclude that no ordered motions

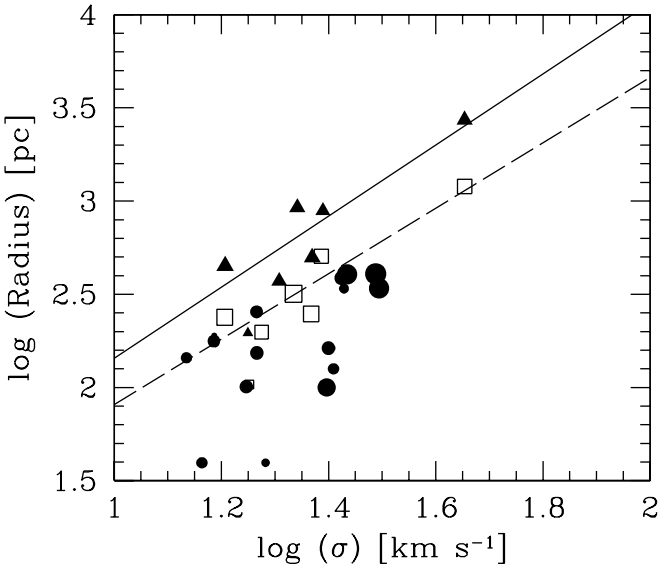

FIG. 4.—Size–line width relation. Symbols show total apertures (*filled triangles*), main knot (*open squares*), and other regions or knots (*filled circles*). Symbol sizes represent relative Hα surface brightness. The lines are simple linear square fits for our data (total: *solid line*; main knot: *long-dashed lines*).

are detected in these galaxies. The measured line widths are unlikely to be due to rotation, because as one goes down to smaller sizes (apertures) one still measures the same σ value (but see Van Zee, Skillman, & Salzer 1998, who reach a different conclusion.)

As mentioned in many previous works about the topic, it is difficult to define a radial scale. Here we consider the aperture size for each extraction of a spectrum that must be a scaled value to the true size of the emitting region. Even though it is noticeable from Figure 4 that there is a clear correlation between size and velocity dispersion for these objects, again, points with low surface brightness seem to fall out of the correlations. There is also a clear similarity between the slopes of the fit to the main knots (Fig. 4, *open squares*, *long-dashed line*) and the total galaxy points (*filled triangles*, *solid line*). Both are very close to what one would expect for virialized systems. The results of the fits are given in Table 5. In addition, we note that these results ($R_{\rm total}$ and $R_{\rm main\ knot}$ versus σ) are compatible with the findings of Telles (1995) for the size versus σ relation for H II galaxies, namely, that the effective radius (derived from surface photometry) versus σ relation is a scaled version of the "core" radius (from luminosity profiles) versus σ relation in a sample of about 40 galaxies, while the latter present a smaller scatter.

TABLE 5

R-σ SIMPLE LEAST-SQUARE TO THE TOTAL AND MAIN KNOT APERTURES VERSUS GLOBAL LINE FIT VALUES

	$R \propto y \log(\sigma)$		
APERTURE	y	Φ (pc)	rms
Total.....	1.90 ± 0.46	0.25 ± 0.63	0.126
Main Knot.....	1.75 ± 0.35	0.15 ± 0.49	0.090

5. DISCUSSION

Without a doubt, one of the most intricate issues in the field of giant H II regions, and now also of H II galaxies, is the origin of their supersonic velocity dispersion ($\sigma_{\rm gas} > c_{\rm H\,II}$).

It has long been established that a simple agglomeration of a large number of H II regions cannot lead to the dominant supersonic line profiles, and thus giant H II regions and H II galaxies constitute a different class of objects. They are different not only because of the size of their emitting regions and the fact that they are powered by recent violent bursts of star formation, but also because of their essence, their peculiar inner dynamics.

It is now well established that the supersonic line width correlates with the size of the emitting region (size $\propto \sigma^2$) and luminosity ($L \propto \sigma^4$) of the ionized regions (Terlevich & Melnick 1981; Melnick et al. 1987, 1988; Telles & Terlevich 1993). The fact that the correlations are similar to the relations inherent to virialized stellar systems such as globular clusters, spiral bulges, and the cores of elliptical galaxies led Terlevich & Melnick to postulate that giant H II regions and H II galaxies are themselves virialized systems and thus that the measured gas velocity dispersion ($\sigma_{\rm gas}$) should directly relate to their total mass. In their original scenario, Terlevich & Melnick envisaged a gravitational potential that forced the collective motion of clumps of gas to present the supersonic σ values. However, in our sample and in the recent finding, in giant H II regions the massive emitting knots present a relative velocity that is not able to explain the observed supersonic σ values (see Tenorio-Tagle et al. 1993, 1996, and references therein). Instead, the brightest knots present an intrinsic value of σ formerly ascribed to the whole ionized region. This fine-tuning regarding the size of the supersonic σ region and its luminosity has brought the empirical correlations into a much better agreement with what is expected from a virialized system. From a theoretical point of view, virialization is now believed to have much to do with the motion of low-mass stars moving in the gravitational potential of the system while undergoing winds. This enhances their cross section and enables them to cause stirring of the gas left over from the star formation event (see Tenorio-Tagle et al. 1993).

On the other hand, some authors have claimed that the supersonic line widths could result from a plethora of unresolved expanding shells caused by the mechanical energy of the large number of massive stars powering each of the sources (see Chu & Kennicutt 1994, and references therein). In the latter case, however, there is no obvious way to explain the empirical correlations, and thus it has been argued that the measured line widths follow the correlations simply due to a lack of resolution in the integrated spectra obtained from single-aperture observations (but see also Tenorio-Tagle et al. 1996).

Our results confirm and extend the empirical correlations found for giant H II regions and H II galaxies. This fact has profound implications both for the observations of H II galaxies and for the interpretation of their supersonic line width. Enhanced spectral and spatial resolution seems to unveil an intricate structure in H II galaxies. Note that the previously measured (single-aperture) supersonic motions in fact arise from regions of much smaller dimension than that occupied by the full extent of the ionized gas. As shown in Figures 3 and 4 for compact H II galaxies, accurate deter-

minations of the size and luminosity of the region presenting the supersonic σ values nicely outline the correlations. H II galaxies, when resolved, present several emitting knots with a variety of shapes, luminosities, and σ values. However, we have shown that in these cases the global integrated value agrees very closely with the properties derived for the main emitting knot. This is simply because the intrinsic properties (luminosity, velocity dispersion) of a galaxy are dominated by the central (core) component.

A fine calibration of these relations for local H II galaxies may be of great importance if used as a distance indicator of galaxies at large redshift, since H II galaxies are easy to find at great distances (see also Melnick, Terlevich, & Terlevich 2000). In particular, because the global line-emitting properties reflect the intrinsic properties of the central core component, observations even with poor spatial resolution could accurately define the luminosity and σ values of the dominant central core in every galaxy.

We thank Roberto Terlevich for a critical reading of the original version of this paper and for valuable discussions on this work. This study was partly financed by the Spanish Dirección General de Enseñanza Superior (DGES), grant PB97-0158. G. T. T. acknowledges partial support from Conacyt (México; grant 211290-5-28501E). G. T. T. and C. M. T. acknowledge the hospitality of the Observatório Nacional (Rio, Brazil) where part of this work was carried out. The WHT is operated on the island of La Palma by the ING at the Observatorio del Roque de los Muchachos. Finally, we thank the anonymous referee for his/her comments that helped improve the presentation of our results.

REFERENCES

Bosch, G. 1999, Ph.D. thesis, Cambridge Univ.
Cairós, L. M., Vilchez, J. M., González-Pérez, J. N., Iglesias-Páramo, J., & Caon, N. 2000, ApJS, in press
Chu, Y.-H., & Kennicutt, R. 1994, ApJ, 425, 720
Doublier, V., Comte, G., Petrosian, A., Surace, C, & Turatto, M. 1997, A&AS, 124, 405
Fuentes-Masip, O., Muñoz-Tuñón, C., Castañeda, H. O., & Tenorio-Tagle, G. 2000, AJ, 119, 2166
Marlowe, A. T., Meurer, G. R., & Heckman, T. M. 1999, ApJ, 522, 183
Melnick, J. 1979, ApJ, 228, 112
Melnick, J., Moles, M., Terlevich, R., & Garcia-Pelayo, J. M. 1987, MNRAS, 226, 849
Melnick, J., Terlevich, R., & Moles, M. 1988, MNRAS, 235, 297
Melnick, J., Terlevich, R., & Terlevich, E. 2000, MNRAS, 311, 629
Muñoz-Tuñón, C. 1994, in Violent Star Formation: From 30 Doradus to QSOs, ed. Tenorio-Tagle (Cambridge: Cambridge Univ. Press), 25
Muñoz-Tuñón, C., Gavryusev, V., & Castañeda, H. 1995, AJ, 110, 1630
Muñoz-Tuñón, C., Tenorio-Tagle, G., Castañeda, H., & Terlevich, R. 1996, AJ, 112, 1636
Noeske, K. G., Guseva, N. G., Fricke, K. J., Izotov, Y. I., Papaderos, P., & Thuan, T. X. 2000, Ap&SS, in press
Sabalisck, N., Tenorio-Tagle, G., Castañeda, H., & Muñoz-Tuñon, C. 1995, ApJ, 444, 200
Sargent, W. L. W., & Searle, L. 1970, ApJ, 162, L155
Schulte-Ladbeck, R. E., Hopp, U., Crone, M. M., & Greggio, L. 1999a, ApJ, 525, 709
Schulte-Ladbeck, R. E., Hopp, U., Greggio, L., & Crone, M. M. 1999b, AJ, 118, 2705
Suntzeff, N. B., et al. 1999, AJ, 117, 1175
Taylor, C. L. 1997, ApJ, 480, 524
Telles, E. 1995, Ph.D. thesis, Cambridge Univ.
Telles, E., & Maddox, S. 2000, MNRAS, 311, 307
Telles, E., & Sampson, L. 2000, Ap&SS, in press
Telles, E., & Terlevich, R. 1993, Ap&SS, 205, 49
———. 1995, MNRAS, 275, 1
———. 1997, MNRAS, 286, 183
Telles, E., Melnick, J., & Terlevich, R. 1997, MNRAS, 288, 78
Telles, E., Tapia, M., Terlevich, R., Kunth, D., & Sampson, L. 1999, in Proc. IAU Symp. 193, Wolf-Rayet Phenomena in Massive Stars and Starburst Galaxies, ed. K. A. van der Hucht, G. Koenigsberger, & P. R. J. Eenens (San Francisco: ASP), 622
Tenorio-Tagle, G., Muñoz-Tuñon, C., & Cid-Fernandes, R. 1996, ApJ, 456, 264
Tenorio-Tagle, G., Muñoz-Tuñon, C., & Cox, D. 1993, ApJ, 418, 767
Terlevich, R., & Melnick, J. 1981, MNRAS, 195, 839
Terlevich, R., Melnick, J., Masegosa, J., Moles, M., & Copetti, M. V. F. 1991, A&AS, 91, 285
Van Zee, L., Skillman, E. D., & Salzer, J. J. 1998, AJ, 116, 1186